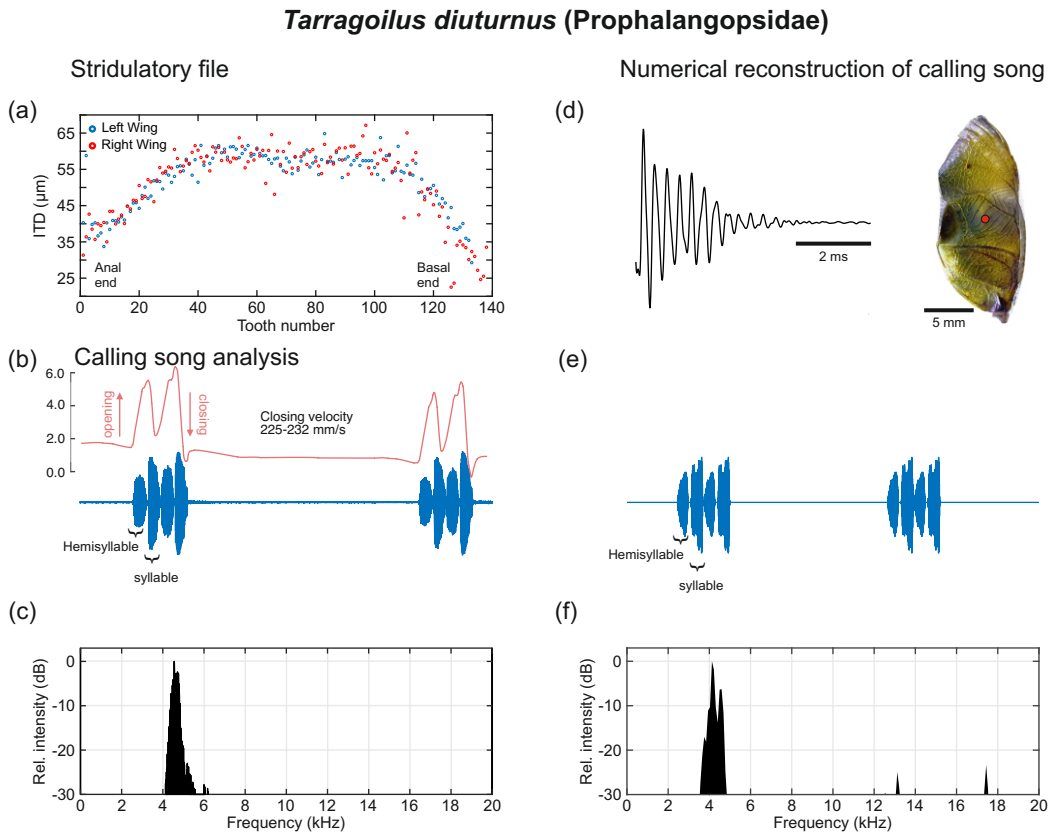

Extended Data Fig. 1. *Tarragoilus diuturnus* (Prophalangopsidae) stridulatory file morphology, calling song and proof-of-concept numerical call reconstruction. **(a)** Tooth distribution on left- and right-wing files (blue and red circles, respectively) of one *T. diuturnus* male. **(b)** Two consecutive calling song chirps (blue oscillogram trace), each containing two syllables. The red line shows the wing motion associated with each syllable. Note that low-amplitude syllables are produced during the opening wing phase, and high-amplitude syllables during the closing phase. **(c)** Power spectrum of the calling song shown in (b). **(d)** Basic oscillation produced by a single tooth-plectrum click on a left wing of *T. diuturnus*. Vibrations were obtained by positioning the LDV laser (red dot) on the main resonant area of the wing while actuating the file using a dissected plectrum of the opposite wing. **(e)** Two consecutive chirps numerically recreated using information from file morphology and tooth-plectrum click shown in (d). (f) Power spectrum of the call shown in (e). disp. = displacement; ITD = inter-tooth-distance.

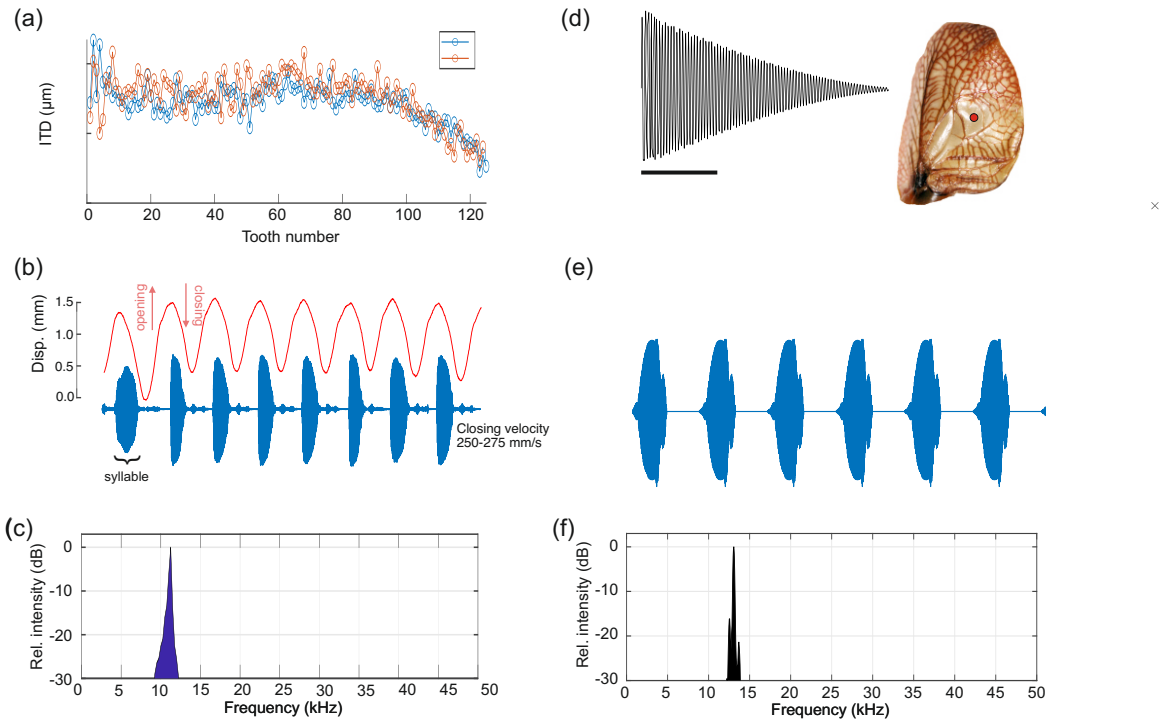

Extended Data Fig. 2. *Cyphoderris monstrosa* (Prophalangopsidae) stridulatory file morphology, calling song and proof-of-concept numerical call reconstruction. **(a)** Tooth distribution on left- and right-wing files (blue and red circles, respectively) of one male. **(b)** Two consecutive calling song sequence(blue oscillogram trace), each containing two syllables. The red line shows the wing motion associated with each syllable. Note that low-amplitude syllables are produced during the opening wing phase, and high-amplitude syllables during the closing phase. **(c)** Power spectrum of the calling song shown in (b). **(d)** Basic oscillation produced by a single tooth-plectrum click on a right wing of a male. Vibrations were obtained by positioning the LDV laser (red dot) on the main resonant area of the wing while actuating the file using a dissected plectrum of the opposite wing. **(e)** Six consecutive calls numerically recreated using information from file morphology and tooth-plectrum click shown in (d). **(h)** Power spectrum of the call shown in (e). disp. = displacement; ITD = inter-tooth-distance.

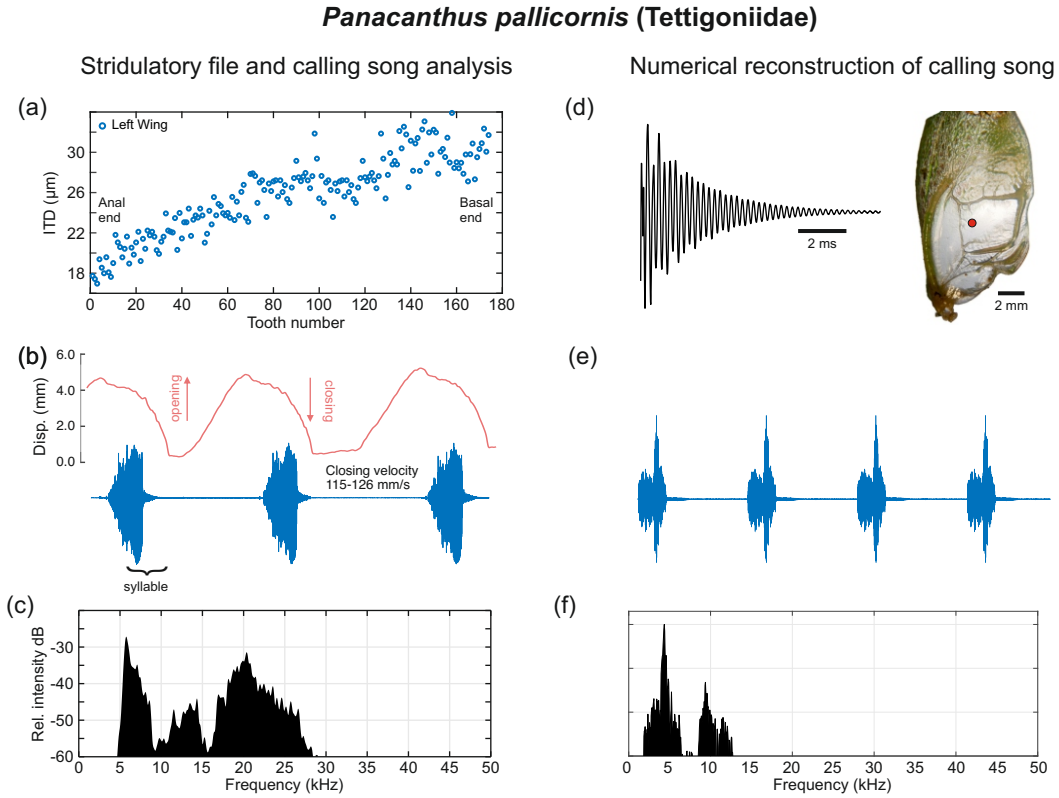

Extended Data Fig. 3. *Panacanthus pallicornis* (Tettigoniidae) stridulatory file morphology, calling song and proof-of-concept numerical call reconstruction. **(a)** Tooth distribution on left (functional) file of one *P. pallicornis* male. **(b)** Three consecutive syllables (blue oscillogram trace) and associated wing motion (red line). Signals are produced during the wing-closing movement; opening of the wing is mostly silent. **(c)** Power spectrum of the syllables in (b). **(e)** Basic oscillation (left) produced by a single tooth-plectrum click on a right wing (right) of *P. pallicornis*. Vibrations were obtained by positioning the LDV laser (red dot) on the main resonant area of the wing while actuating the file using a dissected plectrum of the opposite wing. **(e)** Reconstructed syllable. **(f)** Power spectrum of the artificial call shown in (e). disp. = displacement; ITD = inter-tooth-distance.

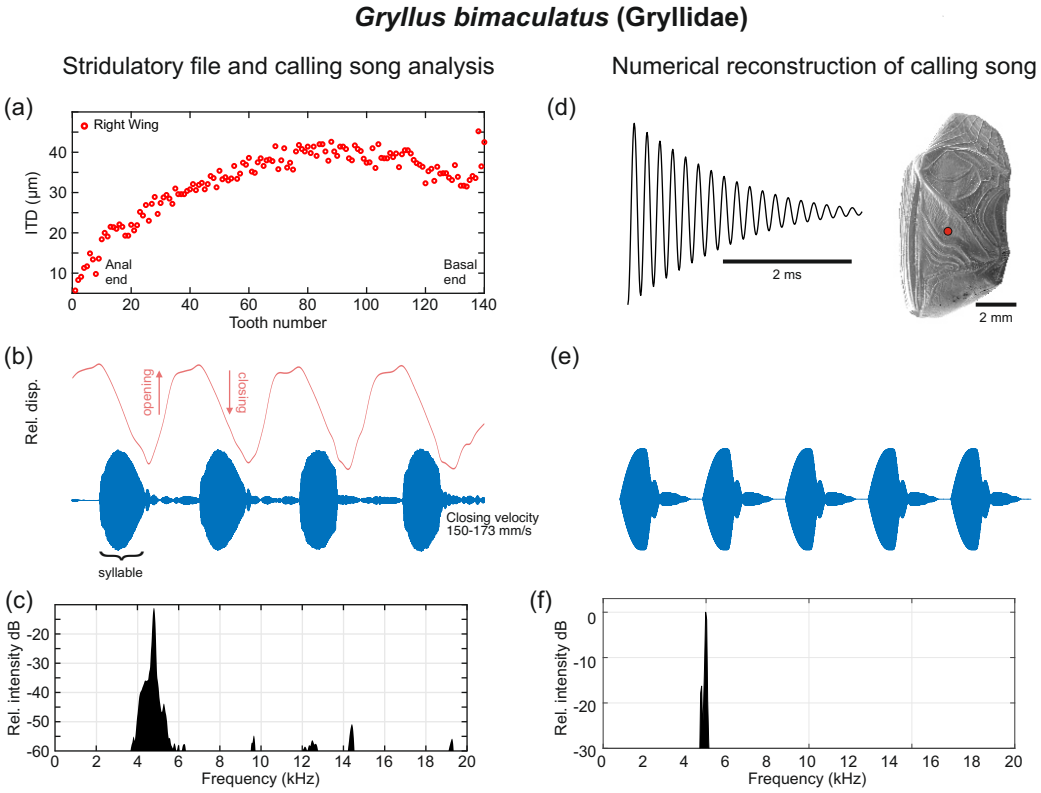

Extended Data Fig. 4. *Gryllus bimaculatus* (Gryllidae) stridulatory file, calling song and proof-of-concept numerical call reconstruction. **(a)** Tooth distribution of right (functional) file of one *G. bimaculatus* male. **(b)** One chirp, containing four syllables (blue oscillogram trace) and associated wing motion (red line). Signals are produced during the wing-closing movement. **(c)** Power spectrum of the syllables in (b). **(d)** Basic oscillation (left) produced by a single tooth-plectrum click on a right wing (right) of *G. bimaculatus*. Vibrations were obtained by positioning the LDV laser (red dot) on the main resonant area of the wing while actuating the file using a dissected plectrum of the opposite wing. **(e)** Reconstructed chirp containing four syllables. **(h)** Power spectrum of the artificial call shown in (e). disp. = displacement; ITD = inter-tooth-distance.

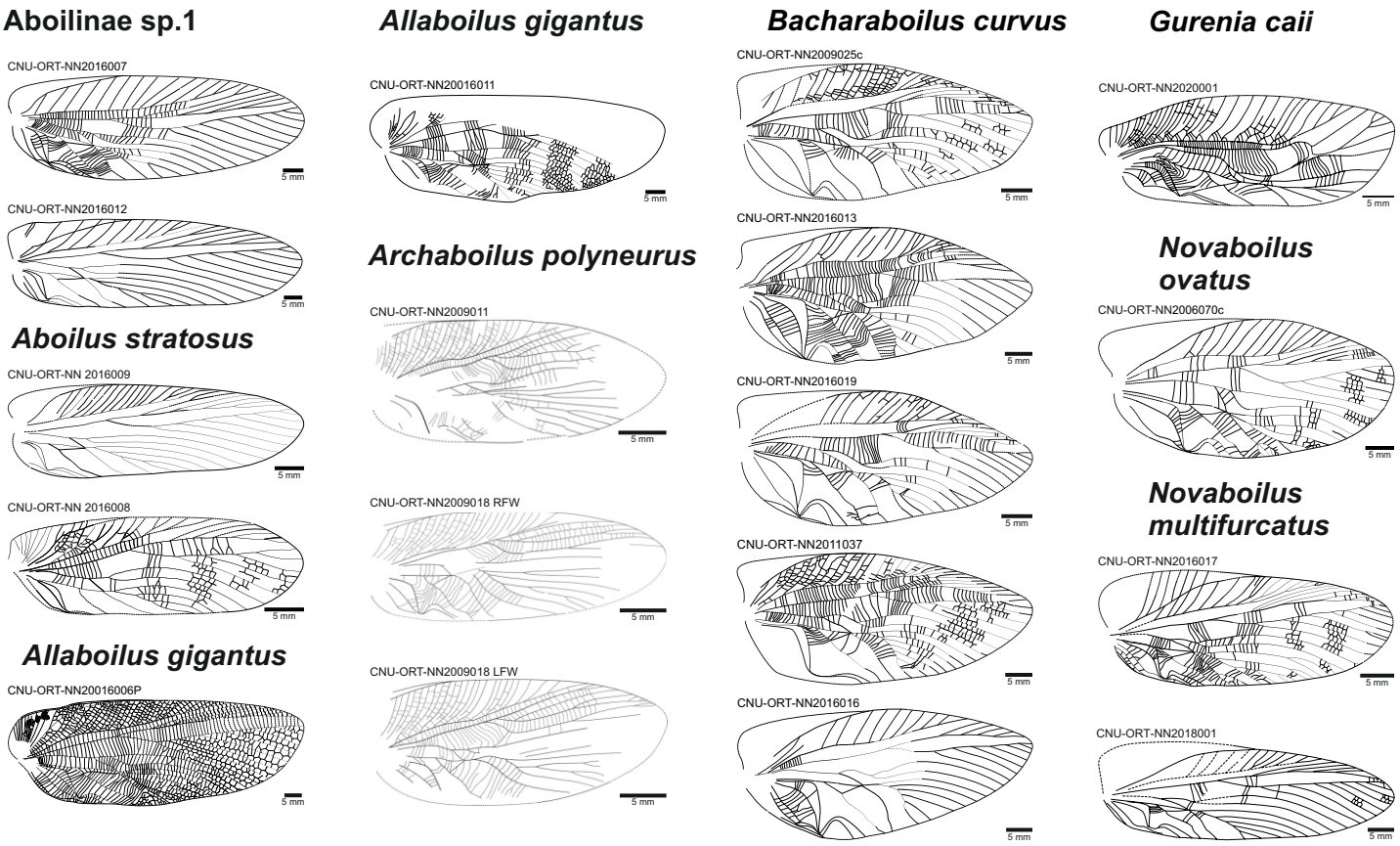

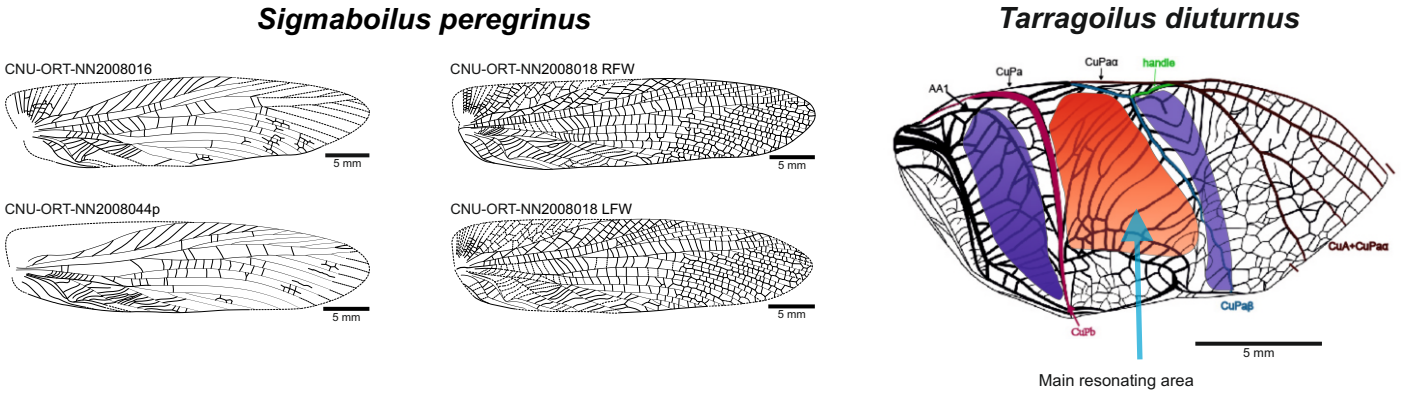

Extended Data Fig. 5. Line drawings of male Prophalangopsidae and Haglidae forewing fossils used in this study. A line drawing of the right wing of *T. diuturnus* (Prophalangopsidae) is presented here for comparison purposes.

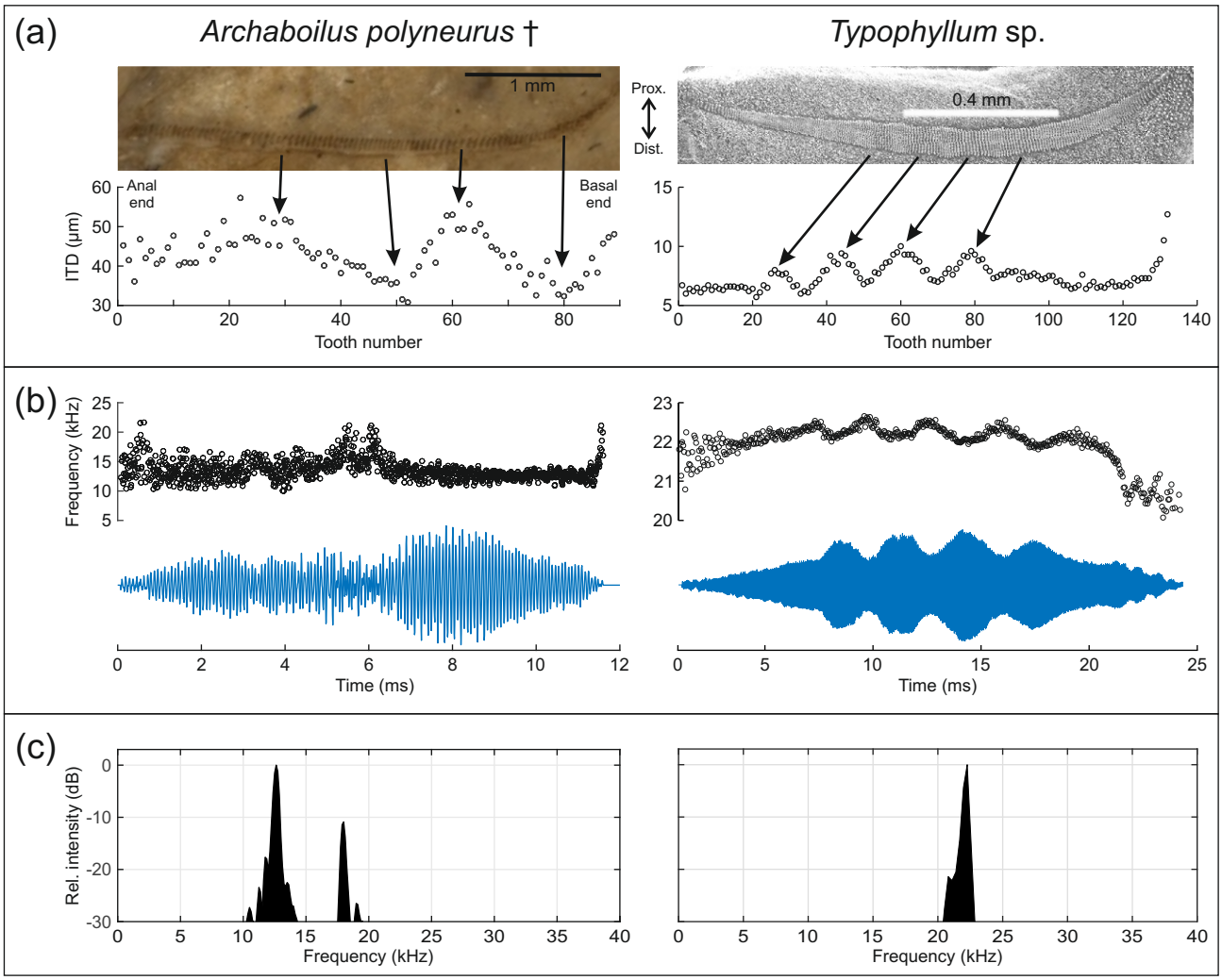

Extended Data Fig. 6. Frequency modulation produced by file morphology in extinct (†) and living katydids: *Archaboilus polyneurus* (Haglidae, left) and *Typophyllum* sp. (Tettigoniidae, Pterochrozinae, right). **(a)** Stridulatory file morphology (top) and inter-tooth-distances (ITD; bottom). Arrows highlight areas of high ITDs. Prox.: proximal; Dist.: distal. **(b)** One syllable (blue oscillogram trace; bottom) created during the closing movement of the wings and thus the striking of subsequent teeth from anal to basal. Top trace: Zero-crossing frequency analysis of the syllables below. Note the effect of tooth arrangement on the instantaneous frequency (and, especially in *Typophyllum*, the amplitude) of the syllable. **(c)** Power spectra of the syllables in (b).

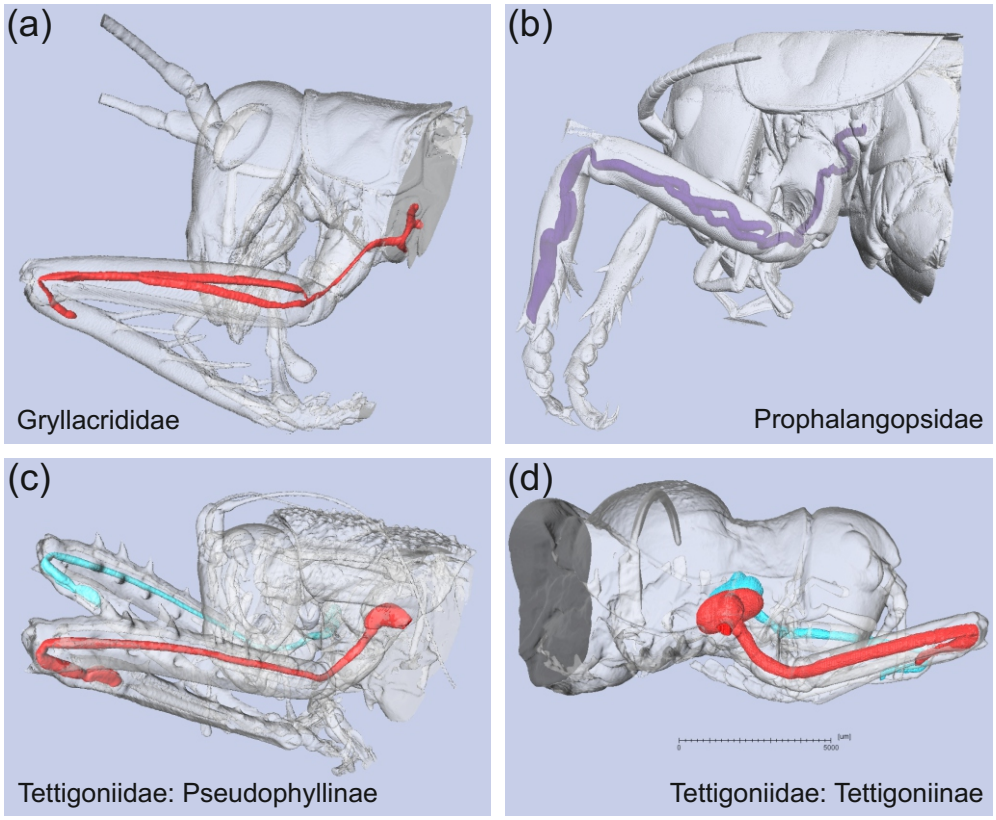

Extended Data Fig. 7. The foreleg trachea and its different functions. **(a)** A bifurcated trachea in a species of Gryllacrididae *(Magnumtergalis* sp.), an atympanate family without known acoustic communication. **(b)** A bifurcated trachea in a living (tympanate) Prophalangopsidae *Tarragoilus diuturnus*. This trachea is unspecialised for sound capture, transmission or amplification. **(c-d)** Different forms of acoustic tracheae (or ear canals) in two Tettigoniidae subfamilies (c) Choeroparnops fulvus (Pseudophyllinae), and (d) *Phymonotus jacintotops* (Tettgoniinae) showing two different forms acoustic trachea.

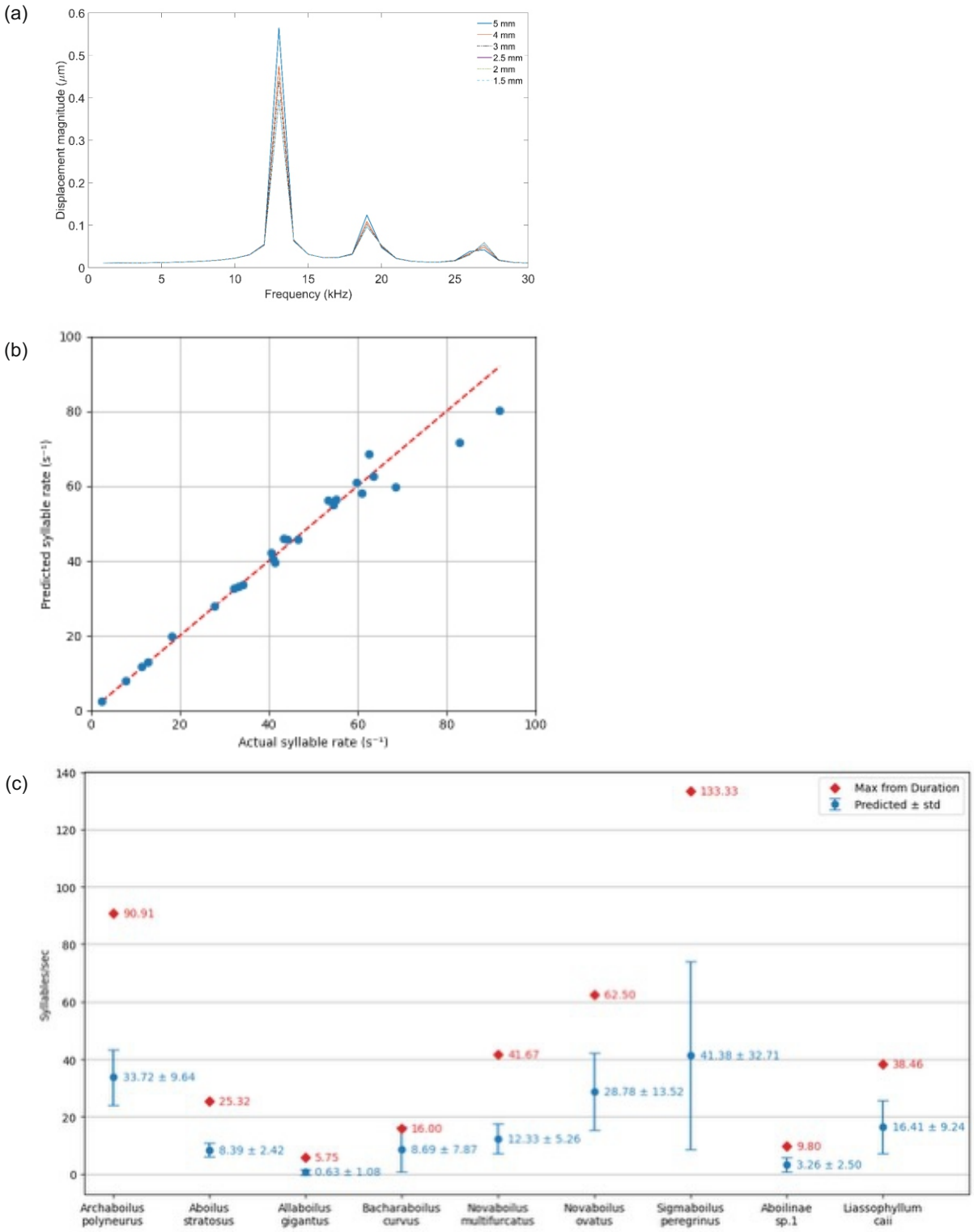

Extended Data Fig. 8. (a) The mesh sensitivity analysis results for *Archaboilus polyneurus*. (b) : Actual vs Predicted syllable rates from Gaussian Process Regression. The dashed red line indicates the ideal fit (y = x). (c) Predicted syllable rates for nine fossil insect species using Gaussian Process Regression. Blue markers indicate the mean predicted syllable rate for each species, with vertical error bars representing standard deviation. Red markers denote the maximum syllable rate for each species.

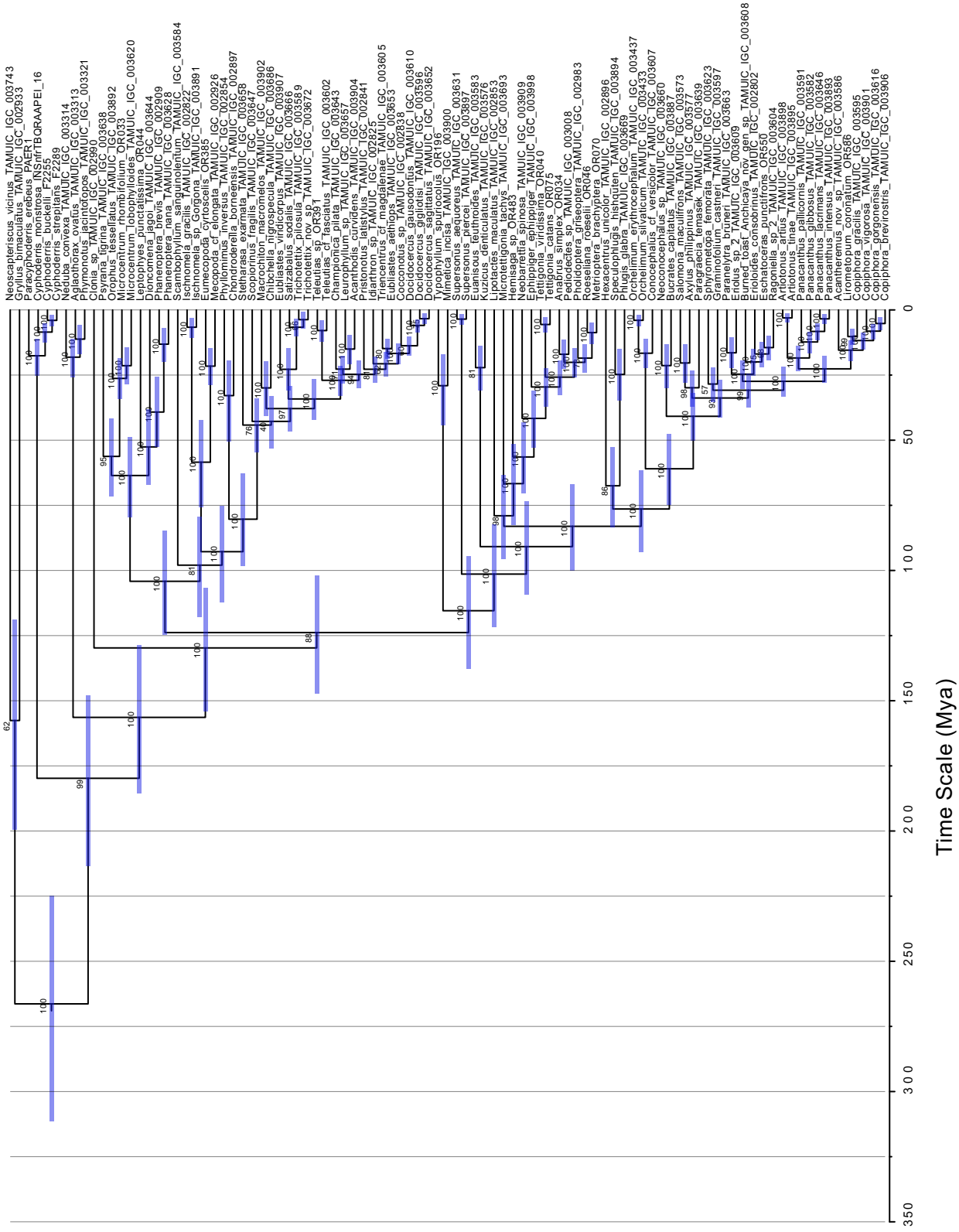

Extended Data Fig. 9. Time-calibrated phylogeny of Ensifera from divergence-time estimation. Node ages are posterior means estimated from combined post–burn-in samples of converged MCMCtree chains, with blue bars showing 95% HPD credible intervals (Mya). Maximum-likelihood bootstrap support values are overlaid on the corresponding nodes. The full taxon set was dated to maximize temporal inference, then the tree was pruned to the subset of taxa with acoustic data for downstream comparative analyses.

Extended data, Table 1. Predictions of carrier frequency for existing and newly presented fossil Ensifera, as well as two extant members of the Prophalangopsidae not included in the phylogeny, from OLS regressions (least informed approach), PGLS regressions (more informed approach), and phylogenetically informed predictions (most informed approach). Note that all previous predictions lie within the error range for the phylogenetically informed approach, while OLS and PGLS alone vary in their predictions.

Species	Family	File length	Node position	OLS	PGLS	Phylo-informed ± SE	Previous predictions	Reference
Archaboilus polyneurus †	Haglidae	4	98	10.56	7.38	9.75 ± 4.66	n/a	This study
Aboilus stratosus †	Prophalangopsidae	4	102	10.56	7.38	11.34 ± 5.20	n/a	This study
Allaboilus gigantus †	Prophalangopsidae	9.3	102	4.73	3.42	5.24 ± 2.41	n/a	This study
Bacharaboilus curvus †	Prophalangopsidae	9.2	102	4.78	3.46	5.30 ± 2.43	n/a	This study
Novaboilus multifurcatus †	Prophalangopsidae	5.1	102	8.38	5.91	9.08 ± 4.17	n/a	This study
Novaboilus ovatus †	Prophalangopsidae	8	102	5.46	3.93	6.02 ± 2.76	n/a	This study
Sigmaboilus peregrinus †	Prophalangopsidae	2.1	102	19.48	13.26	20.42 ± 9.37	n/a	This study
Aboilinae sp.1	Prophalangopsidae	7.2	102	6.04	4.32	6.62 ± 3.04	n/a	This study
Gurenia caii †	Haglidae	7.8	98	5.59	4.02	5.30 ± 2.53	n/a	This study
Eomortoniellus handlirschi †	Tettigoniidae	1.36	149	29.44	19.69	26.75 ± 8.71	32	Woodrow et al.[33]
Pseudotetigonia leona †	Tettigoniidae	4.2	106	10.08	7.06	11.19 ± 4.13	6.5	Greenwalt & Rust[5]
Archaboilus musicus †	Haglidae	9.34	98	4.71	3.41	4.49 ± 2.15	6.4	Gu et al.[4]
Pseudotetigonia amoena †	Tettigoniidae	4.2	106	10.08	7.06	11.19 ± 4.13	7.0	Rust et al.[6]
Prophalangopsis obscura	Prophalangopsidae	10.3	99	4.30	3.12	4.11 ± 2.00	4.7	Woodrow et al.[33]
Tarragoilus diuturnus	Prophalangopsidae	7.0	99	6.20	4.43	4.85 ± 2.79	4.6 (known)	This study

Extended data, Table 2. Wing membrane thickness in relation to eigenfrequency models and phylogenetically informed prediction of carrier frequency (fc) used in COMSOL models for each species. Note the FEA eigenfrequency is not a model prediction, but obtained by adjusting wing thickness until within the range of the phylogenetically informed prediction..

Species	Family	Wing thickness (μm)	FEA obtained eigenfrequency (kHz)	Phylo-informed fc (kHz ± SE)
Archaboilus polyneurus †	Haglidae	7.0	13.1	9.75 ± 4.66
Aboilus stratosus †	Prophalangopsidae	6.5	11.8	11.34 ± 5.20
Allaboilus gigantus †	Prophalangopsidae	18.0	8.8	5.24 ± 2.41
Bacharaboilus curvus †	Prophalangopsidae	10.0	5.0	5.30 ± 2.43
Novaboilus multifurcatus †	Prophalangopsidae	5.5	10.5	9.08 ± 4.17
Novaboilus ovatus †	Prophalangopsidae	6.5	5.6	6.02 ± 2.76
Sigmaboilus peregrinus †	Prophalangopsidae	7.0	20.5	20.42 ± 9.37
Aboilinae sp.1	Prophalangopsidae	10.0	6.0	6.62 ± 3.04
Gurenia caii †	Haglidae	7.0	5.9	5.30 ± 2.53

Extended data, Table 3. Damping (ζ) and Quality factor (Q) measurement for the wings of living Ensifera specimens, using LDV.

	Gryllus bimaculatus	*Cyphoderris monstrosa*	*Tarragoilus diuturnus*	*Panacanthus pallicornis*	*Docidocercus sagittatus*
Wing resonant frequency	4.8 kHz *N=26*	13.5 kHz *N=8*	4.5 kHz *N=10*	5.0 kHz *N=3*	25.0 kHz *N=3*
LW ζ	0.0295696 ± 0.010328	0.036226 ± 0.007575	0.029570 ± 0.008066	0.081738777 ± 0.048247953	0.055495536 ± 0.001196257
RW ζ	0.027596 ± 0.010586	0.041021 ± 0.016782	0.035604 ± 0.014615	0.03453006 ± 0.011626186	0.042616392 ± 0.007486051
Q_3 LW	19.306923 ±7.675369	14.286165 ± 2.694056	19.084877 ± 5.992190	6.097554938±4.988570281	9.012541632 ± 0.195407467
Q_3 RW	20.423077 ± 6.587378	14.212860 ± 6.067572	17.903415 ± 11.819217	15.54069767±4.788834981	11.98269936 ± 2.146699289

Extended data, Table 4. Material properties implemented in the numerical models of the fossilised wings

Wing Material Properties	Constant value	References
Young's Modulus (GPa)	9	Smith et al. [76] Woodrow et al.[33] Vincent & Wegst[138]
Density (kg/m^3)	1200	Vincent & Wegst[138] Woodrow et al.[33]
Poisson's Ratio	0.33	Jafarpour et al.[139] Woodrow et al.[33]